Active Contour Without Edges

Report by: Neelesh Verma *
Guide: Prof. Allen Tannenbaum **
(*neverma, **arobertan @cs.stonybrook.edu)
Department of Computer Science, Stony Brook University

May 2023

Abstract

Image Segmentation has always been one of the challenging tasks in computer vision with its applications in medical imaging, remote sensing, robotics, surveillance, etc. There have been many mathematical models originating as early as the 1970s. Chan-Vese segmentation is one of the models that doesn't consider edges into account when solving the segmentation problem. However, the original proposed Chan-Vese algorithm was for 2 phase segmentation and grayscale images. In this report, we'll look at the original Chan-Vese and its extensions to multi-phase segmentation and RGB images.

1 Introduction

We can define the task of segmentation to divide the image into multiple segments. Active Contour has been a very common framework for this task. They are designed to solve problems where the approximate shape of the boundary is known. Essentially, it is an energy-minimizing, deformable spline influenced by constraint and image forces that pull it towards object contours and internal forces that resist deformation. In images, these energies come from features, like lines and edges.

One of the basic ideas in active contours is to evolve a curve, have some stopping condition for that curve, and thus segment the image or detect some objects. In classical active contour models, generally, this stopping condition is the edge detector, i.e., stop the curve motion once the edge is detected. Consider an image u_0, we can define our edge detector function g as

$$g(|\nabla u_0|) = \frac{1}{1 + |\nabla G_\sigma * u_0|^2} \tag{1}$$

where G is Gaussian filter with some σ to smooth the image. The curve evolves by a variant of the mean curvature motion [8] having this edge function as an extra factor in the velocity. On the edges, the gradient will tend towards infinity and this function will approach 0, thus stopping the curve motion.

In the case of images, the gradients are discrete and bounded. This poses two major issues with classical active contours based on edges -

1. The gradients are discrete and bounded in the case of images. So the stopping function g will not go to 0 and thus the curve may pass through the edges.

2. For noisy images, the Gaussian smoothing has to be strong, otherwise the noise may get detected as an edge too. However, this smoothing can smooth the edges too.

Chan-Vese paper [1] proposed a novel model based on Mumford-Shah functional for segmentation [6]. This is also an energy minimization problem that can be reformulated as a level-set formulation, leading to an easier way to solve the problem. In this report, we will start with the Mumford-Shah model, its relation to Chan-Vese, the level-set formulation approach for Chan-Vese, and finally some experiments and a few extensions to multi-phase and RGB images.

2 Mumford-Shah Model

Let Ω be a bounded open set of $\mathbb{R}^2$, with $\partial\Omega$ as its boundary. Let f denote a grayscale image on the domain Ω. The Mumford and Shah [6] model approximates the image f by a piecewise smooth function u as the solution to the minimization problem

$$F^{MS}(u, C) = \arg\min \mu\text{Length(C)} + \lambda \int_{\Omega} (f(x) - u(x))^2 dx + \int_{\Omega \backslash C} |\nabla u(x)|^2 dx \quad (2)$$

where C is an evolving curve. The first term in the equation penalizes the length of the separating curves and encourages the creation of simple boundaries between the regions. The second term is a data fidelity term that ensures that the segmented regions match the background or noise of the original image. The third term penalizes image gradients and encourages smoothness in the segmented regions. The Mumford-Shah equation suggests selecting the edge set C as the segmentation boundary. The approximation solution to Mumford-Shah was computed using the Ambrosio– Tortorelli method of Chan-Vese [2].

The algorithms for solving the general Mumford–Shah model tend to be relatively complicated and computationally expensive. They also pointed out a reduced form of this problem which is simply to restrict F^{MS} to piecewise constant functions u, i.e., $u = c_i$, a constant on each connected components R_i of $\Omega \backslash C$. This reduced case is also called as Minimal Partition problem. This simplified version can be written as -

$$F^{MS}(u, C) = \arg\min \mu\text{Length(C)} + \lambda \int_{\Omega} (f(x) - u(x))^2 dx \quad (3)$$

In this case, C is necessarily the boundary of a closed set. However, this minimization problem is non-convex. However, it was proved that there exists a solution to this problem by Mumford and Shah [7]. Later on, a much simpler proof was given by Morel and Solimini [4].

3 Chan-Vese Model

The active contour model of Chan-Vese is a particular case of minimal partition problem, in which, we only look for the best approximation u of f, as taking only 2 values -

$$u = \begin{cases} c_1, \text{average of } u_0 \text{ inside C} \\ c_2, \text{average of } u_0 \text{ outside C} \end{cases} \quad (4)$$

There will be only 1 edge representing C. We can clearly see that Chan-Vese originally applies single-phase segmentation. We will show in the next section how u comes out to be like this.

There is an additional term added that penalizes the enclosed area. So the Chan-Vese method is to find among all u that minimizes -

$$\mu\,\text{Length(C)} + \nu\,\text{Area(Inside(C))} + \lambda_1 \int_{inside(C)} |f(x) - c_1|^2 dx + \lambda_2 \int_{outside(C)} |f(x) - c_2|^2 dx \tag{5}$$

Similar to Mumford-Shah, the first term controls the regularity by penalizing the length. The second term penalizes the enclosed area of C to control its size. The third and fourth terms penalize the discrepancy between the piecewise constant model u and the input image. The segmentation obtained by finding a local minimizer for this problem is the best piece-wise two-phase constant approximation u of the image f. By using the same proof of existence for Mumford-Shah by Morel and Solimini [4], we can also have a proof of existence for Chan-Vese. This model was solved using a level-set formulation, so we will be looking at the level-set formulation of this model in the next section.

An Intuitive Look at the Model

We have already talked about the first 2 terms of equation 5. Let's look at the other 2 terms.

$$F_1(C) = \int_{inside(C)} |f(x) - c_1|^2 dx$$
$$F_2(C) = \int_{outside(C)} |f(x) - c_2|^2 dx$$

The first term can be interpreted as the force to shrink the contour. The second one is responsible for increasing the contour. We can consider the following 4 cases -

Figure 1: Variation of forces F_1 and F_2

When the boundary C is outside the object, then $F_2(C) \approx 0$ because $f(x) \approx c_2$ outside C. Inside the boundary C, there are 2 different values of image - black and grey, therefore, $F_1(C) > 0$.

Similarly, when the boundary is inside the object, $f(x) \approx c_1$, therefore $F_1(C) \approx 0$. Also, when the boundary is half inside and half outside, then both forces will be positive. In this case, the forces will tend to move the curve inside as well as outside (inside for some parts and outside for some parts).

When the evolving curve reaches the actual boundary of the image, then both forces will become 0. It is important to note that we haven't yet considered the effect of parameters λ_1 and λ_2. We can consider these as the strength factor that we want to give to both forces. On increasing one, that particular force will be more strength than the other, changing the final boundaries. In most of the cases, we simply use $\lambda_1 = \lambda_2 = 1$.

4 Level Set Formulation

To solve the minimization problem mentioned in equation 5, we need to minimize overall possible set boundaries C. One easy way to do this is to use the level-set method introduced by Osher and Sethian [9]. Here, we introduce a new function ϕ and define it such that ϕ is 0 on C. Therefore,

$$C = \{x \in \Omega : \phi(x) = 0\} \tag{6}$$

The inside and the outside of C are distinguished by the sign of ϕ. We choose ϕ to be positive inside C and negative outside C.

Also, note that for a given C, there is more than one possible level set representation. If ϕ is a level set function for Ω, then so is any other function ψ having the same sign.

$$\text{sign}(\psi(x)) = \text{sign}(\phi(x)) \tag{7}$$

For level set formulation, we will replace the variable C with the variable ϕ. Provided that ϕ is smooth enough (Lipschitz continuous) and indeed a distance function, we can replace term by term of equation 5.

- μ length(C) $= \mu \,.\, \text{length}\{\phi = 0\}$
- ν Area(Inside(C)) $= \nu \,.\, \text{area}\{\phi \geq 0\}$
- $\lambda_1 \int_{inside(C)} |f(x) - c_1|^2 dx = \lambda_1 \int_{\phi \geq 0} |f(x) - c_1|^2 dx$
- $\lambda_1 \int_{outside(C)} |f(x) - c_2|^2 dx = \lambda_2 \int_{\phi < 0} |f(x) - c_2|^2 dx$

Therefore, our new Chan-Vese equation becomes

$$\begin{aligned} F(\phi, c_1, c_2) =& \mu \,\text{length}\{\phi = 0\} + \nu \,\text{area}\{\phi \geq 0\} + \\ & \lambda_1 \int_{\phi \geq 0} |f(x) - c_1|^2 dx \; + \lambda_2 \int_{\phi < 0} |f(x) - c_2|^2 dx \end{aligned} \tag{8}$$

To simplify further, we will need Heaviside function H and it's derivative, Dirac measure δ (concentrated at 0) -

$$H(t) = \begin{cases} 1, & t \geq 0 \\ 0, & t < 0 \end{cases} \tag{9}$$

$$\delta(t) = \frac{d}{dt} H(t) \tag{10}$$

Now, we can simplify the terms of equation 8 even further as -

$$\begin{aligned} \text{length}\{\phi = 0\} &= \int_\Omega |\nabla H(\phi)| dx \ = \int_\Omega \delta(\phi) |\nabla \phi| dx \\ \text{area}\{\phi \geq 0\} &= \int_\Omega H(\phi) dx \end{aligned}$$

The area of the Ω is obtained in the second integral as the integral of $H(\phi)$. The first integral containing the Dirac mass δ is not really an integral, but a curve integral along the boundary C.

Also, the last two terms of equation 8 -

$$\begin{aligned} \lambda_1 \int_{\phi \geq 0} |f(x) - c_1|^2 dx &= \lambda_1 \int_\Omega |f(x) - c_1|^2 H(\phi) dx \\ \lambda_2 \int_{\phi < 0} |f(x) - c_2|^2 dx &= \lambda_2 \int_\Omega |f(x) - c_2|^2 (1 - H(\phi)) dx \end{aligned}$$

Thus, our final Chan-Vese equation after all these simplifications will become -

$$\begin{aligned} F(\phi, c_1, c_2) = \mu \int_\Omega \delta(\phi) |\nabla \phi| dx + \nu \int_\Omega H(\phi) dx + \\ \lambda_1 \int_\Omega |f(x) - c_1|^2 H(\phi) dx \ + \lambda_2 \int_\Omega |f(x) - c_2|^2 (1 - H(\phi)) dx \end{aligned} \tag{11}$$

We can solve the minimization problem of F using Lagrange's multiplier method. First, we differentiate with respect to c_1 -

$$\begin{aligned} \frac{\partial}{\partial c_1} F = 2\lambda_1 \int_\Omega (f(x) - c_1) H(\phi) dx &= 0 \\ \int_\Omega (f(x) - c_1) H(\phi) dx &= 0 \\ c_1 &= \frac{\int_\Omega f(x) H(\phi) dx}{\int_\Omega H(\phi) dx} \end{aligned} \tag{12}$$

Similarly, we can solve for c_2 -

$$c_2 = \frac{\int_\Omega f(x)(1 - H(\phi)) dx}{\int_\Omega (1 - H(\phi)) dx} \tag{13}$$

If we look at c_1 and c_2 closely, they are just averages of f inside and outside the level set.

$$c_1 = \frac{\int_\Omega f(x)H(\phi)dx}{\int_\Omega H(\phi)dx} \quad = \quad \text{the average of } u_0 \text{ in } \{\phi \geq 0\} \tag{14}$$

$$c_2 = \frac{\int_\Omega f(x)(1-H(\phi))dx}{\int_\Omega (1-H(\phi))dx} \quad = \quad \text{the average of } u_0 \text{ in } \{\phi < 0\} \tag{15}$$

Now, if we keep c_1 and c_2 fixed and minimize the energy with respect to ϕ, we obtain the Euler-Lagrange equation for ϕ -

$$\frac{\partial}{\partial t}\phi = \delta(\phi)\left[\mu \text{div}\left(\frac{\nabla\phi}{|\nabla\phi|}\right) - \nu - \lambda_1(f-c_1)^2 + \lambda_2(f-c_2)^2\right] \tag{16}$$

Now, we are good to apply these equations to an image to see the working of Chan-Vese. But before that, we need to look at H and δ again. For theory, these work perfectly fine but we need a slightly regularized version of these 2 functions for images case. This is because they are difficult to use in numerical methods directly. The regularized version helps the model represent the boundaries between the different regions in the image in a smooth and continuous manner.

Regularized version of H and Dirac δ

There have been multiple regularized versions available for H and δ. A commonly used H [11] is -

$$H_\epsilon(x) = \frac{1}{2}\left(1 + \frac{2}{\pi}\arctan\left(\frac{t}{\epsilon}\right)\right) \tag{17}$$

It's derivative δ_ϵ is -

$$\delta_\epsilon(t) = \frac{d}{dt}H_\epsilon(t) = \frac{\epsilon}{\pi(\epsilon^2 + t^2)} \tag{18}$$

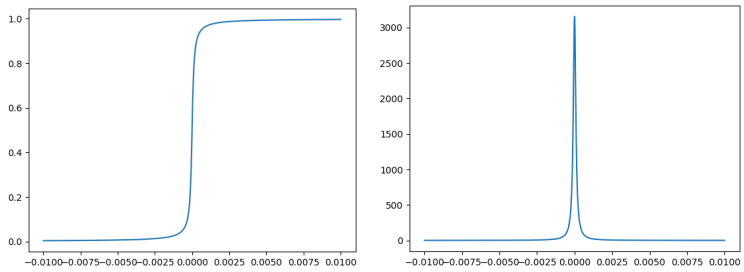

Figure 2: a) Regularized H b) Regularized Dirac

If we look closely at the regularized versions, we can see that they are actually second approximations. There is a very good reason that we didn't use the first approximation. Since our energy equation is non-convex, and the first approximation for δ has very small compact support, the interval $[-\epsilon, \epsilon]$, the iterative algorithm may depend on the initial curve and may not compute global minimizer.

We need to pick some initialization for the contour. A good choice is the function -

$$\phi(x) = \sin(\frac{\pi}{5}x)\sin(\frac{\pi}{5}y) \tag{19}$$

It defines the initial segmentation as a checkerboard image. This initialization has been shown to have fast convergence.

5 Numerical Implementation

We will look at how to implement the method numerically. There are various methods to numerically solve the problem. He and Osher [3] proposed a topological derivative approach, and Badshah and Chan [5] developed a multigrid approach. Here, we will only discuss the original approach as given by Chan and Vese.

Assume that f is sampled on a regular grid $\Omega = \{0, ..., M\} \times \{0, ..., M\}$. The evolution of ϕ is discretized in space according to -

$$\begin{aligned}\frac{\partial \phi_{i,j}}{\partial t} = \delta_\epsilon(\phi_{i,j}) \left[\mu \left(\nabla_x^- \frac{\nabla_x^+ \phi_{i,j}}{\sqrt{\eta^2 + (\nabla_x^+ \phi_{i,j})^2 + (\nabla_y^0 \phi_{i,j})^2}} + \nabla_y^- \frac{\nabla_y^+ \phi_{i,j}}{\sqrt{\eta^2 + (\nabla_x^0 \phi_{i,j})^2 + (\nabla_y^+ \phi_{i,j})^2}} \right) \right] \\ + \delta_\epsilon(\phi_{i,j}) \left[\nu - \lambda_1 (f_{i,j} - c_1)^2 + \lambda_2 (f_{i,j} - c_2)^2 \right]\end{aligned} \tag{20}$$

where $i, j = 1, 2, ..., M-1$, ∇_x^+ denotes the forward difference in the x-dimension, ∇_x^- denotes backward difference, $\nabla_x^0 = (\nabla_x^+ + \nabla_x^-)/2$ is central difference. The same holds for y-direction. η is just to prevent division by 0. Let

$$A_{i,j} = \frac{\mu}{\sqrt{\eta^2 + (\nabla_x^+ \phi_{i,j})^2 + (\nabla_y^0 \phi_{i,j})^2}} \tag{21}$$

$$B_{i,j} = \frac{\mu}{\sqrt{\eta^2 + (\nabla_x^0 \phi_{i,j})^2 + (\nabla_y^+ \phi_{i,j})^2}} \tag{22}$$

then, we can write the discretization as -

$$\begin{aligned}\frac{\partial \phi_{i,j}}{\partial t} &= \delta_\epsilon(\phi_{i,j}) \left[A_{i,j}(\phi_{i+1,j} - \phi_{i,j}) - A_{i-1,j}(\phi_{i,j} - \phi_{i-1,j}) \right] \\ &+ \delta_\epsilon(\phi_{i,j}) \left[B_{i,j}(\phi_{i+1,j} - \phi_{i,j}) - B_{i-1,j}(\phi_{i,j} - \phi_{i-1,j}) \right] \\ &- \delta_\epsilon(\phi_{i,j}) \left[-\nu - \lambda_1 (f_{i,j} - c_1)^2 + \lambda_2 (f_{i,j} - c_2)^2 \right]\end{aligned} \tag{23}$$

On the right-hand side, the first two terms discretize the curvature.

$$\begin{aligned}\text{div}\left(\frac{\nabla \phi}{|\nabla \phi|}\right) &= \partial_x \left(\frac{\partial_x \phi}{\sqrt{(\partial_x \phi)^2 + (\partial_y \phi)^2}} \right) + \partial_y \left(\frac{\partial_y \phi}{\sqrt{(\partial_x \phi)^2 + (\partial_y \phi)^2}} \right) \\ &\approx \nabla_x^- \frac{\nabla_x^+ \phi_{i,j}}{\sqrt{\eta^2 + (\nabla_x^+ \phi_{i,j})^2 + (\nabla_y^0 \phi_{i,j})^2}} + \nabla_y^- \frac{\nabla_y^+ \phi_{i,j}}{\sqrt{\eta^2 + (\nabla_x^0 \phi_{i,j})^2 + (\nabla_y^+ \phi_{i,j})^2}}\end{aligned} \tag{24}$$

We can see a mix of various differences. This is just so that the combined result is centered yet better localized than simply using centered differences for each derivative. In the first term, the numerator $\nabla_x^+ \phi_{i,j}$ is logically centered at $(i+1/2, j)$. The denominator is selected as $(\nabla_x^+ \phi)^2 + (\nabla_y^0 \phi)^2$ so that it, and hence the quotient is centered at (i, j) as desired.

The time is discretized with a Gauss-Sidel method. The values $\phi_{i,j}, \phi_{i-1,j}, \phi_{i,j-1}$ are evaluated at time-steps $n+1$ and all other time-steps n.

$$\frac{\partial \phi_{i,j}}{\partial t} = \frac{\phi_{i,j}^{n+1} - \phi_{i,j}^{n}}{dt} \tag{25}$$

The boundary conditions are enforced by duplicating the pixels near the borders.

$$\phi_{-1,j} = \phi_{0,j}, \quad \phi_{M,j} = \phi_{M-1,j}, \quad \phi_{i,-1} = \phi_{i,0}, \quad \phi_{i,M} = \phi_{i,M-1}$$

We can always reinitialize the level set function after every N iteration by replacing the ϕ with the signed distance function to C or any other function having the same sign at each point. This change does not modify the segmentation boundary itself, but it prevents new components from appearing far away from the current boundary. The termination condition can be to check the difference between two consecutive ϕ and stop if that is below a certain threshold.

6 Experiments

In this section, we will present various results. The whole point of the paper is that the model can detect boundaries without using gradient information.

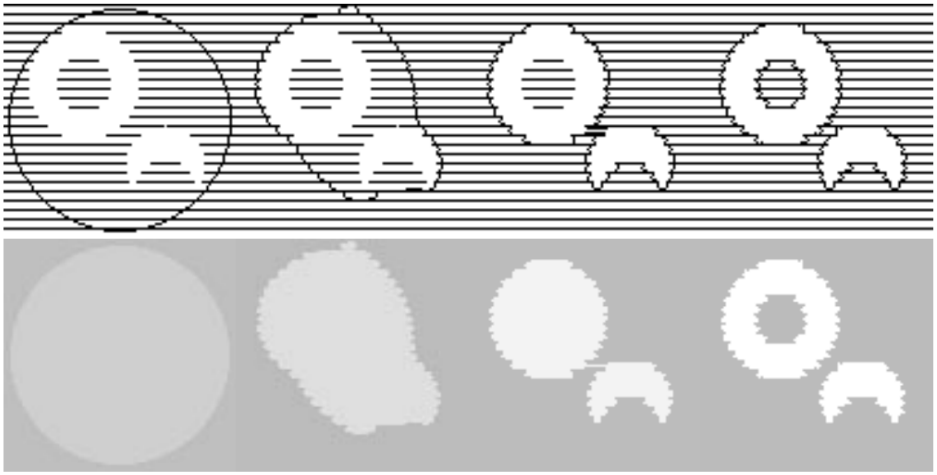

Figure 3: This is to illustrate the fact that the model can detect boundaries without using the gradient. The top row represents evolving contour and the bottom row represents piecewise constant approximations: c_0 and c_1

In figure 3, we can see that the image has various convexities and an interior contour which is automatically detected. Here, we started with a circle as the initial contour. However, the position of the initial contour is not important in this case.

Another good application of Chan-Vese is the case of noisy images. Also, note that the model is able to detect the internal boundary of the torus.

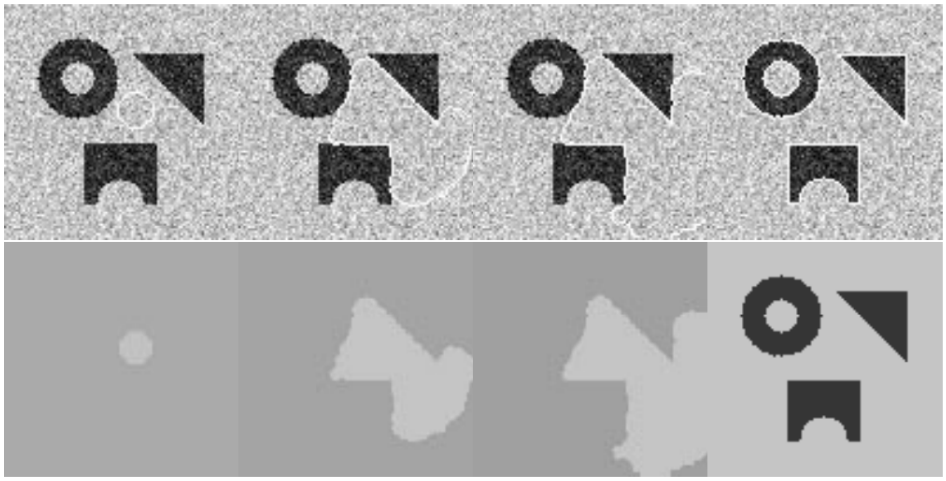

Figure 4: Working of Chan-Vese in case of noisy image

Next, we try on a real image of a heart. We can see in figure 5 that the model is able to separate the chambers but still, both the chambers themselves aren't separated.

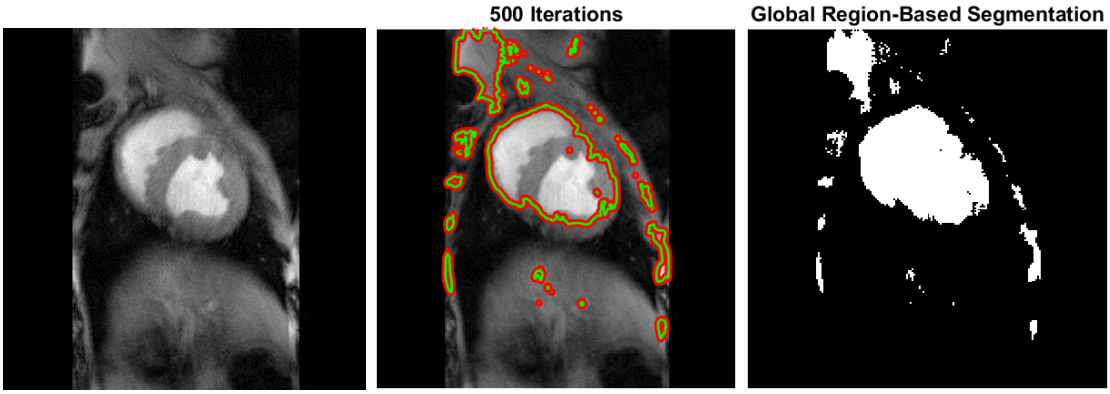

Figure 5: Chan-Vese on a real image of a heart

Let's try one more real image, this time a brain.

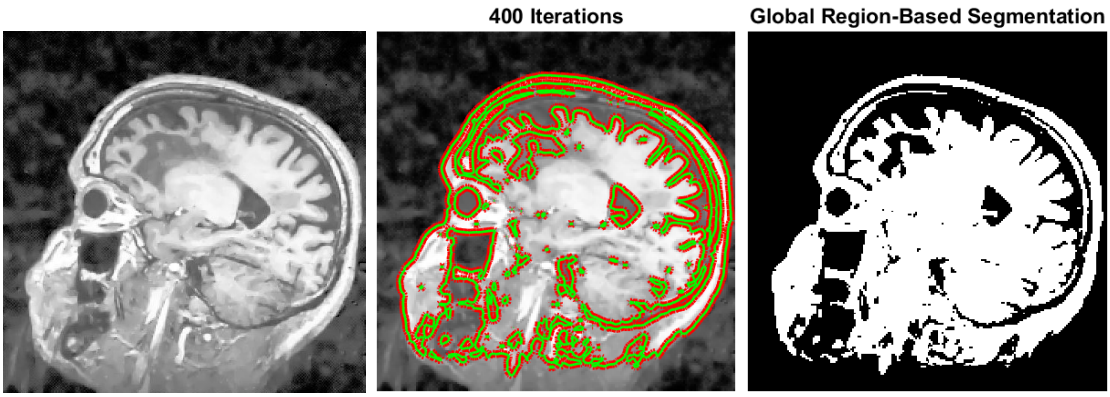

Figure 6: Brain Image segmentation

We can see that for the brain image, the segmentation looks pretty good as it is separating the grey matter. We can also take a look at a random image not related to Medical 7. We have used a checkerboard-based initial contour.

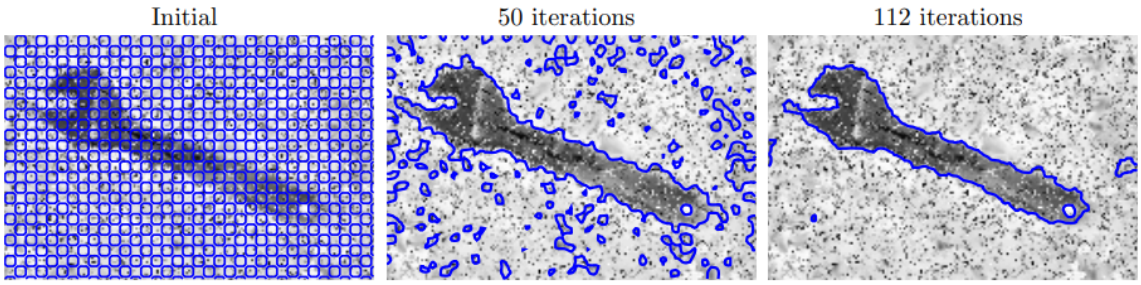

Figure 7: Wrench with a checkerboard initial contour

6.1 Varying the parameter μ

In equation 11, there are 2 important parameters μ and ν. First, we will show the effect of varying μ. It basically controls the length of the curve. So the intuition is that increasing μ will produce smoother boundaries and decreasing μ will give more accurate boundaries but more segmented. The exact same is depicted in figure 8.

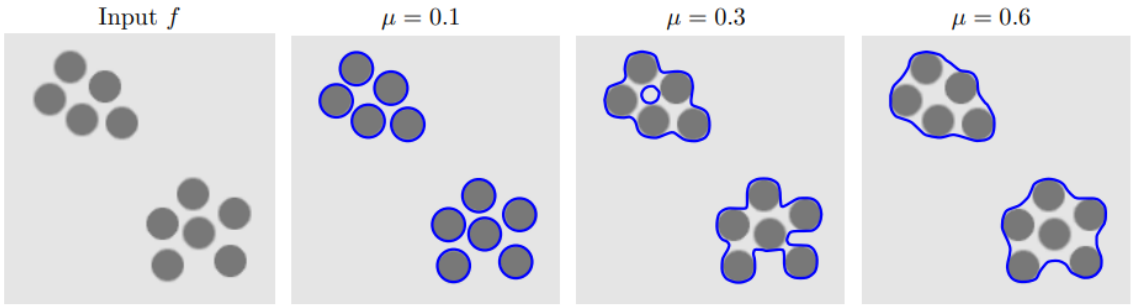

Figure 8: Effect of increasing μ

6.2 Varying the parameter ν

The next parameter to test is ν. Again looking at equation 11, we can see that ν controls the area under the boundary C. So if we increase ν too much, the area inside the boundary C should keep on decreasing and at some point approach 0. This is exactly the case in figure 9.

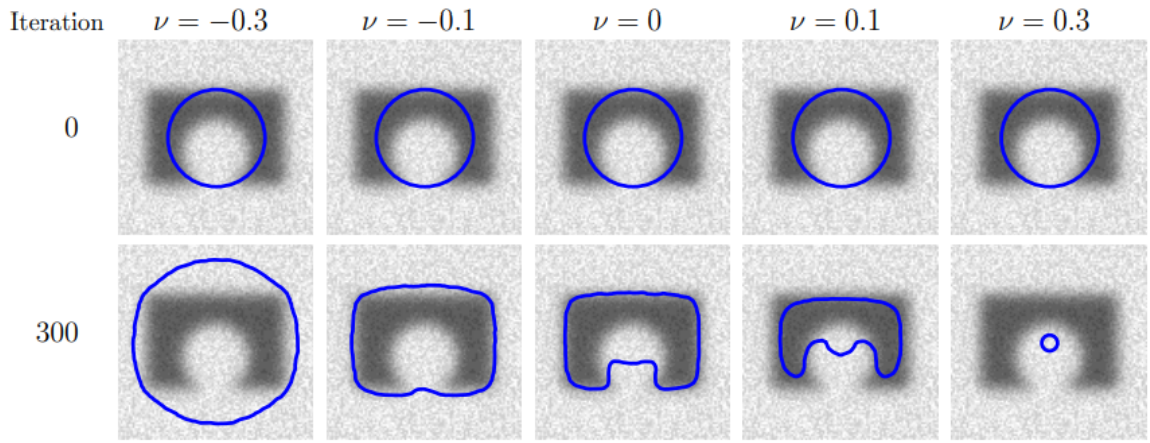

Figure 9: Effect of increasing ν

6.3 Different Initializations

Till now, we have been using some initialization - circle, checkerboard, etc., but we haven't seen if it makes a difference. Let's compare two popular ones - checkerboard and circle.

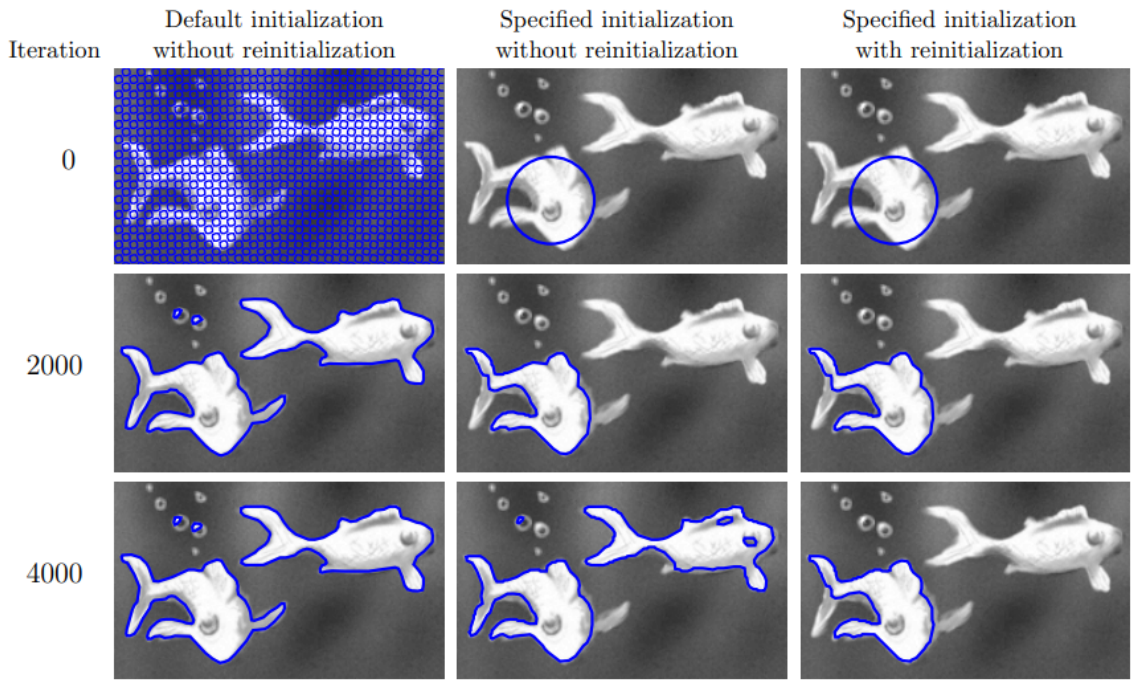

Figure 10: Effect of different initialization and reinitialization

We can control the objects that we want to segment using the initial contour. Reinitialization may need to be used to avoid including separate objects. If we look at the second and third columns, if we reinitialize the contours after 2000 iterations we can avoid the segmentation of the second fish.

6.4 RGB Images Segmentation

Original Chan-Vese works for gray-scale images. However, we can extend it for 3-D images easily. In the section on the intuitive explanation of the model, we have looked that we can view the model as the result of two forces - one pushing the boundary inside and the other pulling outside. If we wish to apply the model to a 3-D image, we can simply apply the model to each of the 2-D images, compute the resultant F_1 and F_2 forces and use the resultant force to move the boundary.

Figure 11: Chan-Vese Extension to RGB Images

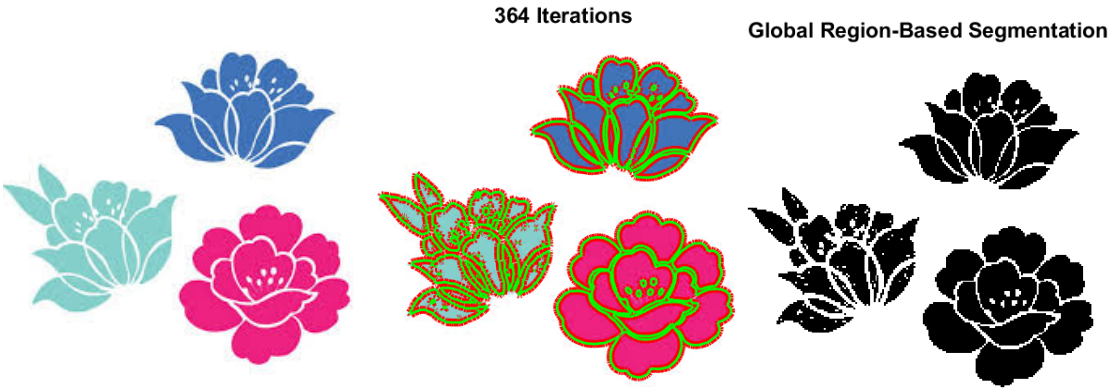

Figure 12: Chan-Vese Extension to RGB Images

6.5 Multi-phase Segmentation

We have looked at only binary segmentation till now. However, we can extend the algorithm for multi-phase segmentation as well. Basically, the algorithm will group the regions to their different mean value and if two regions have a close mean value than other colors, these two colors will be grouped into one. It will be more helpful if we look at a few examples.

Figure 13: Multi-phase Segmentation

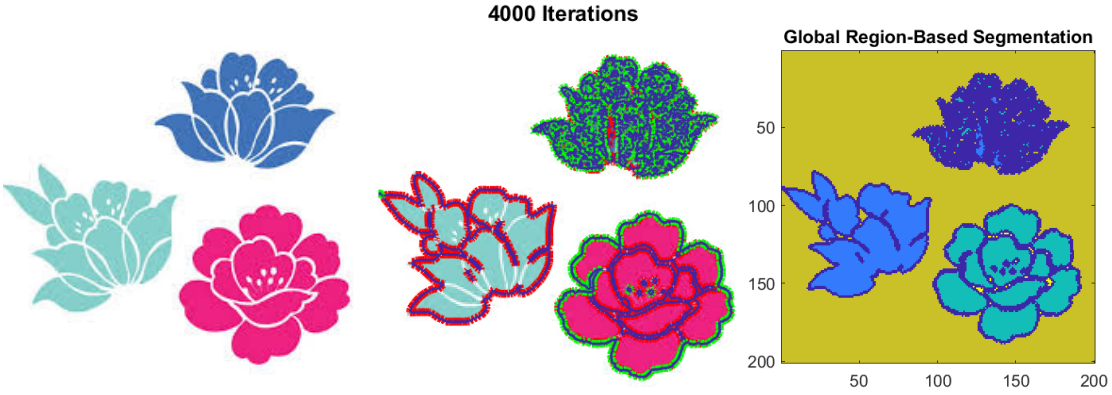

Figure 14: Multi-phase Segmentation

7 Conclusion

In this report, we have looked at the Active Contour model proposed by Chan-Vese, and how it differs from classical active contour models. We can detect objects whose boundaries are not necessarily defined by gradient or with very smooth boundaries. We

also looked at the application of active contours to noisy images. Later, we extended the model to 3-D images and multi-phase segmentation as well. There have been multiple developments based on this model. Tsai, Yezzi, and Willsky [10] developed a general-level set curve evolution framework similar to Chan–Vese. Chan-Vese has given a good base for many segmentation algorithms.

References

[1] T.F. Chan and L.A. Vese. "An Active contour model without edges". In: *IEEE Transactions on Image Processing* 10.2 (2001), pp. 266–277. DOI: 10.1109/83.902291.

[2] T.F. Chan and L.A. Vese. "Reduced non-convex functional approximations for image restoration segmentation". In: *UCLA CAM Reports* (1997).

[3] Lin He and S. Osher. "Solving the Chan-Vese Model by a Multiphase Level Set Algorithm Based on the Topological Derivative". In: *Scale Space and Variational Methods in Computer Vision*. 2007.

[4] Jean-Michel Morel and Sergio Solimini. "Variational Methods in Image Segmentation: with seven image processing experiments". In: 1994.

[5] "Multigrid Method for the Chan-Vese Model in Variational Segmentation". In: *Communications in Computational Physics* 4.2 (2008), pp. 294–316. ISSN: 1991-7120. DOI: https://doi.org/. URL: http://global-sci.org/intro/article_detail/cicp/7791.html.

[6] David Mumford and Jayant Shah. "Optimal approximations by piecewise smooth functions and associated variational problems". In: *Communications on Pure and Applied Mathematics* 42 (1989), pp. 577–685.

[7] David Mumford and Jayant Shah. "Optimal approximations by piecewise smooth functions and associated variational problems". In: *Communications on Pure and Applied Mathematics* 42 (1989), pp. 577–685.

[8] Stanley Osher and James A Sethian. "Fronts propagating with curvature-dependent speed: Algorithms based on Hamilton-Jacobi formulations". In: *Journal of Computational Physics* 79.1 (1988), pp. 12–49. ISSN: 0021-9991. DOI: https://doi.org/10.1016/0021-9991(88)90002-2. URL: https://www.sciencedirect.com/science/article/pii/0021999188900022.

[9] Stanley Osher and James A Sethian. "Fronts propagating with curvature-dependent speed: Algorithms based on Hamilton-Jacobi formulations". In: *Journal of Computational Physics* 79.1 (1988), pp. 12–49. ISSN: 0021-9991. DOI: https://doi.org/10.1016/0021-9991(88)90002-2. URL: https://www.sciencedirect.com/science/article/pii/0021999188900022.

[10] A. Tsai, A. Yezzi, and A.S. Willsky. "Curve evolution implementation of the Mumford-Shah functional for image segmentation, denoising, interpolation, and magnification". In: *IEEE Transactions on Image Processing* 10.8 (2001), pp. 1169–1186. DOI: 10.1109/83.935033.

[11] Hongkai Zhao et al. "A Variational Level Set Approach to Multiphase Motion". In: *Journal of Computational Physics* 127 (1996), pp. 179–195.